

Reprogramming Virus Coat Protein Carboxylate Interactions for the Patterned Assembly of Hierarchical Nanorods

Adam D. Brown, Sangwook Chu, Madhu Kappagantu, Reza Ghodssi, and James N. Culver*



Cite This: *Biomacromolecules* 2021, 22, 2515–2523



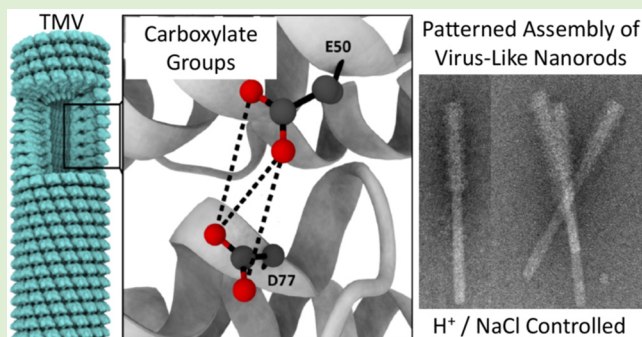
Read Online

ACCESS |

Metrics & More

Article Recommendations

ABSTRACT: The self-assembly system of the rod-shaped tobacco mosaic virus (TMV) has been studied extensively for nanoscale applications. TMV coat protein assembly is modulated by intersubunit carboxylate groups whose electrostatic repulsion limits the assembly of virus rods without incorporating genomic RNA. To engineer assembly control into this system, we reprogrammed intersubunit carboxylate interactions to produce self-assembling coat proteins in the absence of RNA and in response to unique pH and ionic environmental conditions. Specifically, engineering a charge attraction at the intersubunit E50–D77 carboxylate group through a D77K substitution stabilized the coat proteins assembly into virus-like rods. In contrast, the reciprocal E50K modification alone did not confer virus-like rod assembly. However, a combination of R46G/E50K/E97G substitutions enabled virus-like rod assembly. Interestingly, the D77K substitution displays a unique pH-dependent assembly–disassembly profile, while the R46G/E50K/E97G substitutions confer a novel salt concentration dependency for assembly control. In addition, these unique environmentally controlled coat proteins allow for the directed assembly and disassembly of chimeric virus-like rods both in solution and on substrate-attached seed rods. Combined, these findings provide a controllable means to assemble functionally discrete virus-like rods for use in nanotechnology applications.



1. INTRODUCTION

Biologically derived macromolecular assemblies are of increasing interest for their potential in advancing nanotechnology applications. Nucleic acids, proteins, and complexed assemblies of these macromolecules, such as viruses, have been investigated for a wide range of applications including enhanced energy production, sensing, drug delivery, and enzyme sequestration.^{1–4} Interest in these biological components stems from their ability to self-assemble into defined nanoscale structures, to recognize and bind target analytes, to enzymatically catalyze chemical reactions, and to be manipulated genetically, permitting specific modifications to these assemblies. In addition, the bottom-up fabrication strategy afforded by the use of biological components holds the potential to generate novel nanoscale structures and patterns with unique functions. Examples include “DNA origami” that utilizes DNA base pairing to direct the ordered assembly of hundreds of oligonucleotides or the use of protein–protein interaction domains to assemble peptide chains into complex geometric shapes.^{5–8} Combined, these studies represent remarkable initial efforts in the development and application of designed biological assemblies.

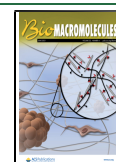
Viruses in the form of virions represent some of the most studied and manipulated naturally occurring submicrometer

self-assembly systems. As such, virus-based assembly systems have been created to encapsidate therapeutics, enzymes, pesticides, and inorganics for use in a range of applications.^{2,9–11} What make viruses particularly amenable to these studies are the molecularly scaled uniform capsid proteins (CP) that, under the appropriate environmental conditions, can be induced to self-assemble into defined nanoscale shapes with great fidelity. In general, modifications of virion assemblies have involved the display of naturally occurring or genetically introduced amino acid residues or functional polypeptide chains that enable the cross-linking of enzymes, nucleic acids, and inorganics to the virion surface.^{1,12–14} These studies add functionality to existing virion structures, but efforts to re-engineer virion assembly to produce novel nanoscale structures are not well developed and in need of additional investigation.

Received: February 26, 2021

Revised: April 7, 2021

Published: April 22, 2021



Some of the most extensive efforts to modify virion assembly have occurred with tobacco mosaic virus (TMV). TMV is a common plant virus prevalent in many environmental systems. The TMV particle consists of ~2130 CP subunits (M.W. 17.5 kDa) packed in an 18 nm diameter helix, the layers of which sandwich a single strand of plus-sense RNA around a 4 nm diameter channel situated along the 300 nm long longitudinal axis.^{15,16} The three-dimensional structure of the CP has been resolved to 2.8 and 2.4 Å for a 20S disk aggregate, consisting of two stacked protein rings, each containing 17 CP subunits^{17,18} and at 2.9 Å resolution for the TMV virion.¹⁶ This comprehensive structural information has led to several innovative assembly systems. Included in these systems is the design of a circular permutant from a rearrangement of the TMV CP with newly created N- and C-termini on the inner rather than outer virion surface, facilitating modifications to the central channel of the virion.¹⁹ In a second system an added cysteine at the inner-channel-proximal CP residue 103 was used to promote the assembly of rod-shaped virus-like particles (VLP) in the absence of viral RNA.²⁰ The disulfide bonds responsible for stabilizing rod assemblies provide a redox-based means to control the production of virus-like protein rods. Alternatively, novel assembly systems have been developed by altering the viral RNA, which plays a critical role as a structural component of the virion.²¹ Specifically, RNAs containing TMV origin-of-assembly sequences (OAs) can be used to direct the assembly of TMV CPs into virus-like rods of defined lengths, into varied CP compositions, or onto patterned substrates.^{22–24} Furthermore, RNA molecules containing multiple OAs can be used to produce branched virion-like structures.²⁵ Combined, these systems provide varying levels of control over the assembly of these virus-based macromolecular assemblies, opening up their potential as functional components in larger and more complex nano- and microscale structures.

Our group has previously developed a VLP assembly system based on the elimination of an assembly destabilizing intersubunit interaction between carboxylate groups.²⁶ Previous studies had identified two sets of carboxylate groups whose intersubunit repulsion provided the driving force for both virus assembly and disassembly.^{16,27–29} The first group is composed of CP residues E50 and D77 interacting between axially adjacent subunits, while the second consists of E106 and E95/E97/D109 interacting between laterally adjacent subunits. Outside a host cell, the relatively low pH of the extracellular environment functions to neutralize these repulsive interactions through protonation as well as via the presence of cations, functioning to stabilize the assembled virion. However, upon entry into the cellular environment, the higher pH of the cellular environment and lower cation concentrations result in the loss of stabilizing protons, leading to the destabilization and disassembly of the virion.^{16,30} It is possible to genetically neutralize these repulsive interactions via replacement of the negatively charged carboxylate residues with corresponding amide residues (E to Q and D to N). These neutralizing substitutions function to stabilize the virion assembly, producing long virion-like rods *in planta*.²⁸ In addition, the double axially interacting-carboxylate substitution E50Q/D77N produces long virion-like rods in bacterial expression systems.²⁶ In this study, the directed modulation of TMV-VLP assembly is investigated as a means to control the production of complex hierarchical nanorods. Genetic modifications of the TMV CP were created to modulate both the CP subunit structure and its electrostatic-charge-based

intersubunit interactions to either strengthen or weaken the ability of CP interfaces to self-associate and to associate with other modified or the unmodified CP. These modifications were created to control the assembly of CP subunits for the production of novel nanorod structures.

2. EXPERIMENTAL SECTION

2.1. TMV CP Expression and Purification. TMV CPs were modified as previously described using a cDNA open reading frame (ORF) that was codon-optimized for expression in *Escherichia coli*.²⁶ CP 3' end specific PCR primers encoding FLAG (DYKDDDDK) or HA (YPYDVPDYA) epitope tags along with a *XhoI* restriction site were used in conjunction with a CP 5' end primer encoding an *NdeI* site to amplify the specified CP ORFs. Restriction digest cloning was used to move the amplified ORFs into the pET21(+) expression vector (MilliporeSigma, Burlington, MA). Additional CP amino acid modifications were generated by sequential PCR using overlapping primers encoding the desired codon alterations. All pET21(+) CP ORFs were sequence-verified prior to transformation into BL21-(DE3) *E. coli* K-12 cells. Cell cultures were grown at 37 °C until reaching an absorbance of 0.5 at a wavelength of 600 nm. Cultures were then induced with 1 mM IPTG incubated at room temperature with shaking overnight. Induced cells were pelleted by centrifugation at 4 °C and lysed by resuspension in Bugbuster HT Protein Extraction Reagent with the addition of Lysozyme as prescribed by the manufacturer's protocol (Novagen, Madison WI). The bacterial lysate was diluted 1:10 with 0.1 M pH 7 phosphate buffer and pelleted by centrifugation at 91 000g for 2 h. The resulting pellet was resuspended in 2 mL of 0.1 M pH 7 phosphate buffer and VLPs separated on a 10–40% sucrose gradient in 0.1 M pH 7 phosphate buffer via centrifugation at 91 000g at 14 °C for 1 h. Gradient-purified VLPs were concentrated by centrifugation at 91 000g for 2 h at 4 °C and resuspended in 0.1 M pH 7 phosphate buffer.

2.2. VLP Assembly Systems. For assembly studies purified CPs were first dialyzed in either 0.1 M Tris buffer adjusted for the desired pH or ultrapure water using Spectra/Por dialysis membrane (MWCO: 12–14 000, Spectrum Laboratories, Rancho Dominguez, CA). For generation of extended TMV-VLP complexed particles with distinct and ordered longitudinal components, TMV and CPs were dialyzed either separately or in admixture to solution conditions, promoting disassembly of the VLP CP and then returning to conditions promoting its assembly, either by dialysis or by the addition of concentrated solution.

For assembly of D77K-HA CP onto TMV, 50 μL of a solution containing 3 mg/mL D77K-HA CP and 0.6 mg/mL TMV in 0.1 M pH 7 sodium phosphate buffer was dialyzed as described above first to 0.1 M pH 7 Tris buffer, then to 0.1 M pH 9 Tris buffer to disassemble the D77K CP, and then to 0.1 M pH 7 Tris buffer to initiate reassembly of the D77K CP onto the TMV rod end with each dialysis step taking place overnight at 4 °C. For samples treated with RNase, 0.5 μL of a 1 mg/mL stock solution of RNase A was added to the solution after the dialysis to pH 9 and incubated for 30 min at 37 °C before proceeding with dialysis back to pH 7.

For assembly of R46G/E50K/E97G-FLAG onto TMV, a 50 μL solution containing 1 mg/mL R46G/E50K/E97G-FLAG CP and 0.5 mg/mL TMV in 0.1 M pH 7 sodium phosphate buffer was dialyzed first to 0.1 M pH 7 Tris buffer. The mixture was then dialyzed to filtered ultrapure water brought to pH 7 with NaOH and then to 0.1 M pH 7 Tris buffer with 0.3 M NaCl to initiate assembly of R46G/E50K/E97G CP onto the TMV rod end with each dialysis step taking place overnight at 4 °C.

2.3. Immunolabeling and Electron Microscopy. For immunomicroscopy studies, coassembled TMV and CP samples were adsorbed onto Formvar-coated Ni TEM grids that were subsequently washed with phosphate buffered saline (PBS: 10 mM sodium phosphate, 150 mM NaCl, pH 7). Surfaces were blocked with Blocking Solution for Goat Antibodies (Aurion, Wageningen, The Netherlands). Primary antibodies (anti-FLAG antibodies produced in rabbit, anti-HA antibodies produced in mouse, Sigma-Aldrich, St.

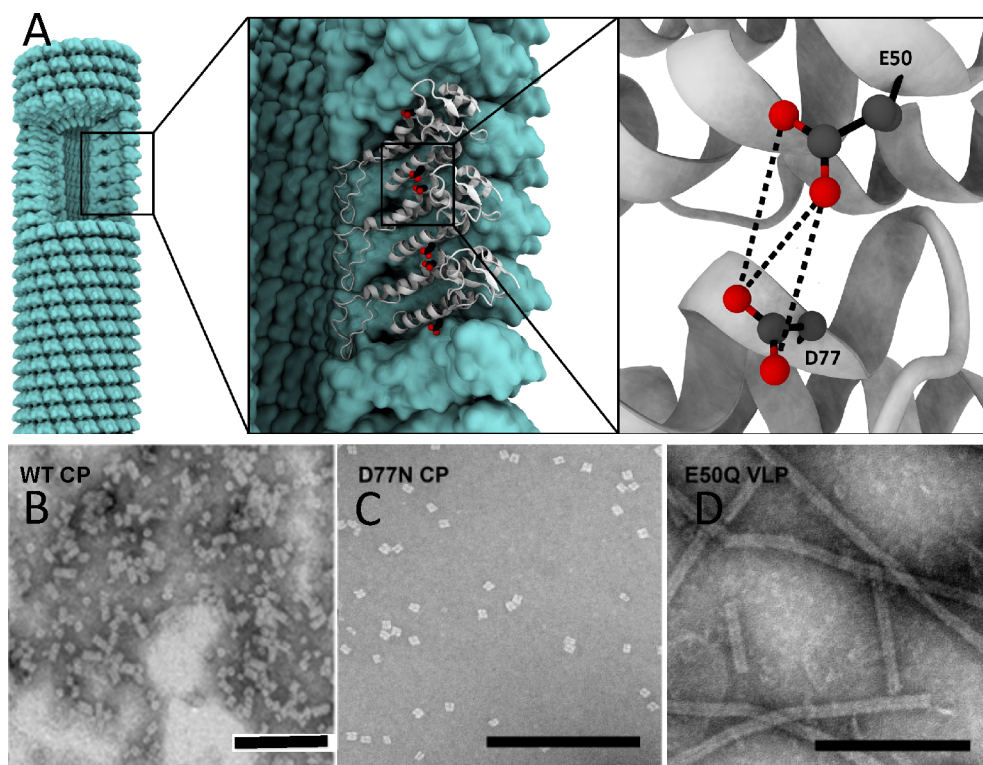


Figure 1. Impact of the axial carboxylate interaction on TMV assembly. (A) TMV virion model with a section removed and sequential enlargements showing the location of the E50 to D77 intersubunit interaction. (B–D) Electron micrographs showing the assembly status of bacterially expressed unmodified TMV CP, TMV D77N CP, and E50Q TMV CP under pH 7.0 conditions. Bars = 100 nm.

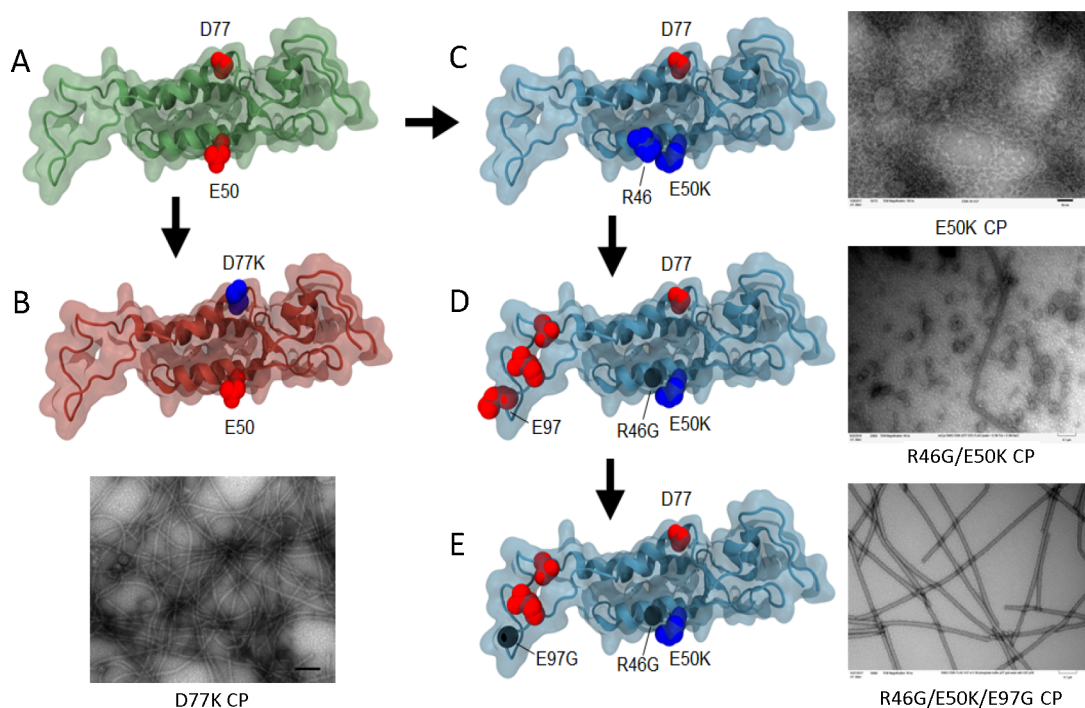


Figure 2. Locations of TMV CP modifications with corresponding micrographs of assembly products. (A) Unmodified TMV CP containing negatively charged axial carboxylates D77 and E50. (B) The D77K CP alone can induce rod production. (C) The E50K substitution fails to produce rods likely due to repulsive interactions with neighboring R46. (D) The R46G/E50K substitutions negate this repulsive interaction, allowing limited rod-like assemblies. (E) The addition of an E97G modification aimed at enhancing lateral intersubunit interactions produces R46G/E50K/E97G CP, which induces virus-like rod production.

Louis, MO) were diluted 1:500 in an incubation buffer (PBS with 0.1% Tween-20 and 0.1% Aurion BSA-c) as needed and applied to

grids at room temperature for 2 h or at 4 °C overnight. Grids were washed three times with 50 μ L drops of incubation buffer. Grids were

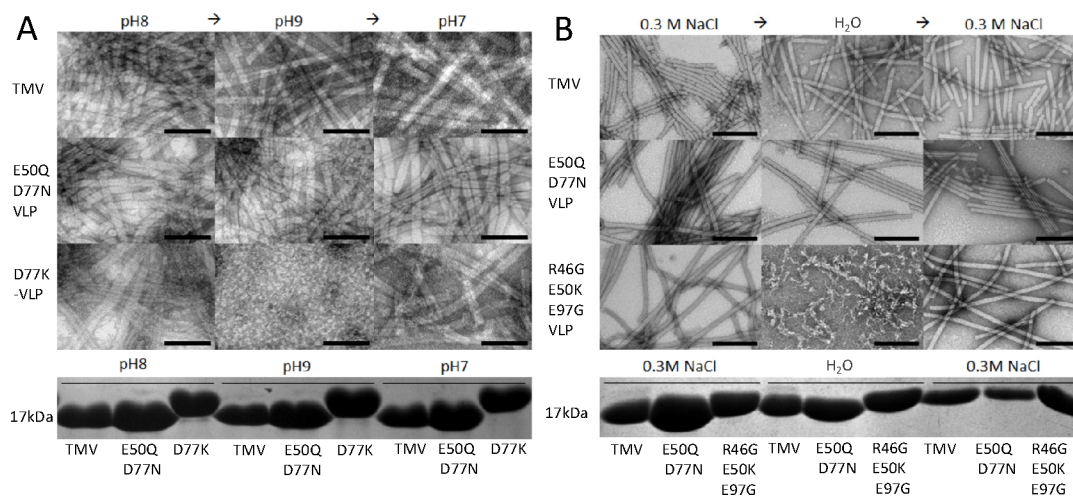


Figure 3. Solution assembly dynamics for carboxylate-altered TMV CPs. (A) TEM images of TMV (top row), E50Q/D77N VLP (middle row), and D77K-HA (bottom row) samples dialyzed sequentially to pH 8, 0.1 M Tris (left column), then to pH 9, 0.1 M Tris (middle column), and finally pH 7, 0.1 M Tris (right column). (B) TEM images of TMV (top row), E50Q/D77N VLP (middle row), and R46G/E50K/E97G-FLAG CP (bottom row) samples dialyzed sequentially to high ionic-strength conditions (0.3 M NaCl, 0.1 M Tris) (left column), then to low solute, deionized water (middle column), and finally returning to high ionic-strength conditions (0.3 M NaCl, 0.1 M Tris) (right column). Lower panels display SDS-PAGE analysis of CP levels under each solution condition. Bars = 100 nm.

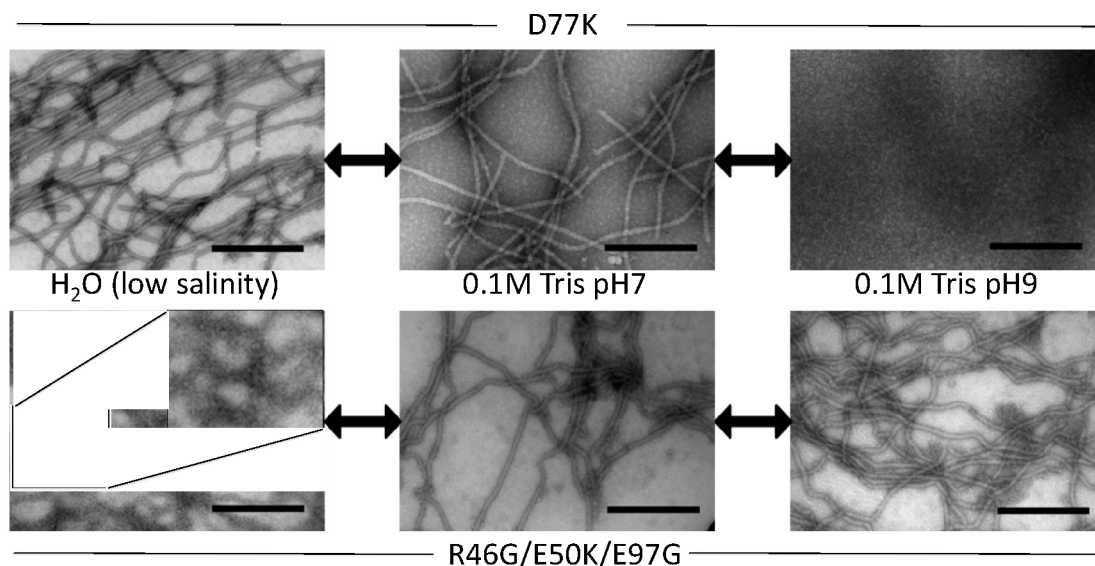


Figure 4. Unique differences in the solution assembly characteristics of carboxylate-altered CPs. (A) D77K-HA and (B) R46G/E50K/E97G-FLAG TEM images showing both variants exist in an assembled state as elongated VLP rods after dialysis in 0.1 M pH 7 Tris (center images). After dialysis with filtered water, D77K-HA CP shows retention of the assembled VLP structure (top left), while R46G/E50K/E97G-FLAG shows a significant loss of assembly structure (bottom left with a magnified box). In contrast, dialysis of the samples from 0.1 M pH 7 Tris (center column) to pH 9 (right column) triggers the complete loss of the virus-like particle structure in D77K-HA CP (top right), while R46G/E50K/E97G-FLAG CP retains its assembly structure. Bars = 200 nm.

stained with 2% uranyl acetate for 1 min and samples imaged using a Zeiss transmission electron microscope at 80 kV.

2.4. Surface-Bound Fabrication of Coassembled Nanoparticles. Gold-coated silica wafers (0.5 cm × 1 cm), cleaned by sequential 5 min submersions in acetone, methanol, and isopropanol with agitation, were spotted with 3 μ L of a 0.1 mg/mL solution of TMV1cys in 0.1 M pH 7 sodium phosphate buffer and allowed to air-dry as previously described.³¹ For assembly onto surface-attached TMV1cys, a 1 mg/mL solution of D77K-HA CP was first predialyzed to 0.1 M Tris pH 9 to promote disassembly with 2 μ g of predialyzed CP added to wafers submerged in 1 mL of 0.1 M Tris buffer, pH 9 or pH 7. The R46G/E50K/E97G-FLAG CP, 1 mg/mL, was predialyzed against filtered water adjusted to pH 7 by addition of NaOH and 2 μ g of the CP added to wafers submerged in 1 mL of either 0.1 M Tris

buffered saline, pH 7 (0.2 M NaCl), or filtered water, pH 7. Wafers were incubated overnight at room temperature and washed three times with the corresponding assembly buffer followed by the addition of anti-FLAG or anti-HA antibodies (Sigma-Aldrich, St. Louis, MO) in 0.1 M Tris buffer saline, pH 7. After 2 h of incubation at room temperature, wafers were washed three times in 0.1 M Tris buffer saline, pH 7, and incubated for 2 h with alkaline phosphatase conjugated secondary antibodies. After a final three times wash, wafers were submerged in 1 mL of substrate buffer (0.1 M pH 7 Tris, 0.2 M NaCl, and 5 mM MgCl) containing 0.15 mg/mL 5-bromo-4-chloro-3-indoyl phosphate and 0.3 mg/mL NitroBT.

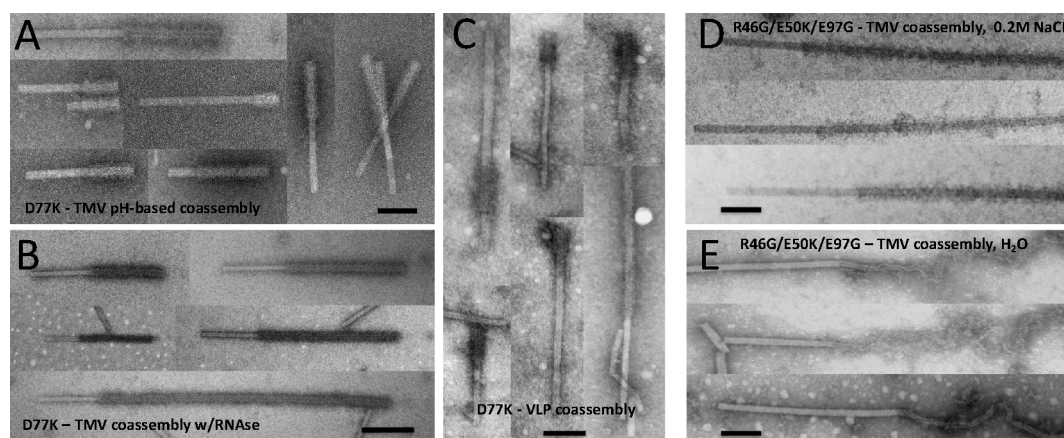


Figure 5. Solution-directed coassembly of carboxylate-altered CPs. (A) TEM images of longitudinally ordered TMV–D77K-HA hybrid nanorods resulting from pH-based VLP disassembly/reassembly. Samples were dialyzed against a pH 9 solution of 0.1 M Tris buffer and then back to pH 7 followed by immunolabeling with anti-HA antibody. (B) RNAase-treated TMV prior to pH-directed assembly with D77K-HA CP, indicating that any exposure of the viral 5' end RNA is not required for coassembly. (C) D77K-HA CP assembled onto a RNA-free VLP-based nanorod produced by the neutralization of the lateral carboxylate cluster, further demonstrating that the viral RNA is not required for coassembly. (D) TEM images of ionic-strength-based R46G/E50K/E97G-FLAG coassembly with TMV. Samples were dialyzed against deionized water and then back to 0.2 M NaCl followed by immunolabeling with anti-FLAG antibody. (E) Coassembled TMV with R46G/E50K/E97G-FLAG washed with deionized water after immunolabeling showing loss of VLP assembly structure. Bars = 200 nm.

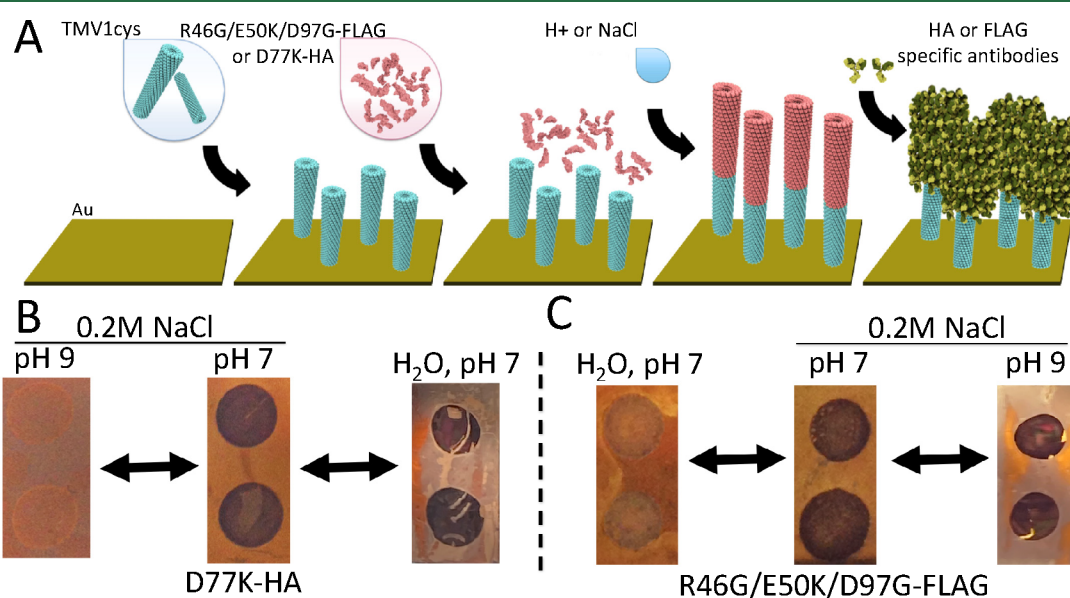


Figure 6. Controlled surface assembly of carboxylate-altered CPs. (A) Diagram displaying assembly steps for the pH or NaCl directed coassembly of D77K-HA and R46G/E50K/E97G-FLAG onto surface-attached TMV1cys. In step 1 TMV1cys is end-attached to a gold-coated silicon chip via a thiol–gold bond. In step 2, disassembled carboxylate-modified CPs are added to the TMV1cys-attached chips. Step 3 involves the incubation of disassembled CPs under specific pH and salt buffer conditions that promote CP assembly onto the exposed end of the attached TMV1cys. Step 4 demonstrates the addition of a primary-tag-specific antibody (FLAG or HA) followed by the addition of a secondary alkaline-phosphatase-conjugated antibody that upon substrate addition produces a dark precipitant on the surface of the gold-coated chip. Chips are thoroughly washed after steps 1, 3, and 4. (B) The pH 7 chip, center, represents two TMV1cys attachment spots showing the directed coassembly of D77K-HA onto attached TMV1cys under pH 7 buffer conditions. The pH 9 chip, left, shows how subsequently incubating a similar D77K-HA coassembled chip in pH 9 buffer leads to the disassembly and loss of the D77K-HA CP, while incubation in the deionized water, right chip, shows no disassembly of D77K-HA CP. (C) The center 0.2 M NaCl chip shows the directed coassembly of R46G/E50K/E97G-FLAG onto the surface-attached TMV1cys under salt conditions. The deionized water chip, left, shows a similar coassembled chip subsequently incubated under no-salt conditions, displaying the disassembly and loss of the R46G/E50K/E97G-FLAG CP from the TMV1cys. The pH 9 chip, right, shows disassembly of R46G/E50K/E97G-FLAG CP from TMV1cys does not occur in a pH-dependent manner.

3. RESULTS AND DISCUSSION

3.1. Reprogramming of the Axial Intersubunit Carboxylate Cluster. Previous studies have identified TMV CP intersubunit carboxylate residues whose repulsive intersubunit interactions play a key role in virion assembly and

disassembly.^{16,29,32} For examination of the contributions of the axial E50–D77 repulsive interaction during nanorod assembly, individual neutral amide substitutions of E50Q and D77N were investigated for their ability to assemble into virus-like nanorods (Figure 1A). Results indicated that at pH 7 the

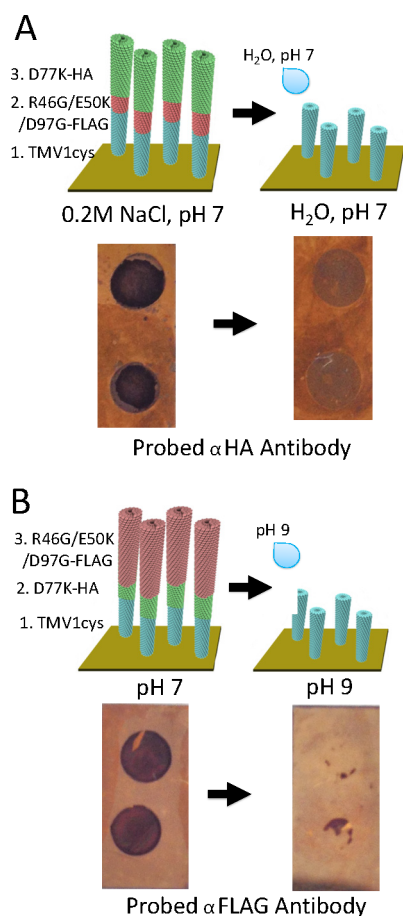


Figure 7. Layered assembly of carboxylate-altered CPs. (A) Top panel diagram for the sequential assembly of, step 1, surface-attached TMV1cys followed by, step 2, the addition and coassembly of R46G/E50K/E97G-FLAG CP in 0.2 M NaCl pH 7 buffer, and then, step 3, coassembly of D77K-HA CP in pH 7 buffer. Lower panel shows two gold-coated chips, each with two TMV1cys attachment spots. Sequentially assembled chips were probed with anti-HA antibody as described in Figure 6. The chip on the left was incubated in 0.2 M NaCl pH 7 buffer, conditions that promote the stability of both R46G/E50K/E97G-FLAG and D77K CPs. The chip on the right was incubated in deionized water, pH 7, conditions that result in the disassembly of R46G/E50K/E97G-FLAG CP but not the D77K-HA CP. The inability to detect assembled D77K-HA CP on the deionized-water-treated chip indicates that disassembly of the R46G/E50K/E97G-FLAG CP layer also results in the loss of the D77K-HA CP layer. (B) Upper panel diagram for the sequential coassembly onto, step 1, surface-attached TMV1cys, followed by, step 2, D77K-HA CP in pH 7 buffer, and finally, step 3, coassembly with R46G/E50K/E97G-FLAG CP in 0.2 M NaCl pH 7 buffer. Lower panel with two coassembled gold-coated chips, each with two TMV1cys attachment spots probed with anti-FLAG antibody. Prior to antibody incubation, the chip on the left was incubated in 0.2 M NaCl pH 7 buffer, conditions that maintain the stability of both D77K-HA and R46G/E50K/E97G-FLAG CPs. The chip on the right was incubated in 0.2 M NaCl pH 9, conditions for the disassembly of D77K-HA CP but not the R46G/E50K/E97G-FLAG CP. The inability to detect assembled R46G/E50K/E97G-FLAG CP on pH 9 treated chips indicates that disassembly of the D77K-HA CP layer also results in the loss of the R46G/E50K/E97G-FLAG CP layer.

D77N mutation produces only two-layer disks, similarly to the unmodified CP (Figure 1B,C). In contrast, the E50Q substitution alone was sufficient to confer assembly of virion-like nanorods (Figure 1D). On the basis of the helical assembly

structure of the TMV virion, D77 is stabilized by a salt bridge with R71 in the same subunit.²⁹ It is likely that the loss of this stabilizing interaction via the D77N mutation leads to the localized disruption of the α -helix where D77 resides, preventing the helical subunit ordering required for the assembly of extended VLP rods. In contrast, E50 is stabilized by an intersubunit interaction with R134 of a neighboring subunit.²⁹ The E50Q substitution would thus not disrupt its localized α -helix structure, leaving the neutralized intersubunit interaction with D77 to drive assembly of the helical VLP nanorod. These results are also consistent with previous findings that the E50Q mutation significantly reduces TMV infectivity and disrupts *in vitro* translation of the embedded RNA genome, presumably by blocking virus disassembly, while the D77N substitution alone does not.²⁸

3.2. Charge–Charge Modifications for Directed Nanorod Assembly. The ability of the axial carboxylate group to control VLP assembly made it an ideal site for further modifications aimed at controlling CP assembly. Initial modifications were directed toward the creation of novel salt bridges between the E50 and D77 carboxylate pairs through the directed replacements with either D77K or E50K (Figure 2A). Interestingly, the D77K substitution resulted in the assembly of rod shaped VLPs (Figure 2B). Structural modeling of D77K indicated sufficient rotational space within the subunit interface at residue 77 to accommodate the lysine residue with its terminal amine group positioned within 3 Å of an opposing E50 carboxyl group from a neighboring subunit. The close approach of the D77K to E50 interaction would result in a new intersubunit salt bridge that is of sufficient strength to counter the localized α -helical disruptions that prevented the D77N from assembling into VLP nanorods.

In contrast, the E50K replacement did not produce helical rod assemblies (Figure 2C). Structural modeling indicates the potential for repulsive electrostatic interference between the lysine substituted for residue E50 and residue R46 situated on the adjacent α -helical turn in the same subunit. For elimination of the presumed electrostatic interference of R46 and accommodation of the E50K substitution, an additional substitution of glycine for R46 was made, generating the R46G/E50K CP variant. Expression of this variant produced only limited rod assemblies, suggesting incomplete compensation of the E50K substitution (Figure 2D). For improvement of assembly stability and VLP formation, a third targeted substitution, E97G, aimed at partially neutralizing the laterally interacting intersubunit carboxylates present in the long inner loop was added to create R46G/E50K/E97G. The E97G substitution stabilizes the long inner loop in a virion-like configuration that promotes the helical ordering of subunits necessary for rod assembly.^{16,28} This triple mutant was found to produce VLP nanorods in quantities and lengths (>1 μm) that were similar to those observed for D77K mutation (Figure 2E). This is consistent with the stabilization of the rod assembly via the new axially placed intersubunit salt bridge and stabilized CP long inner loop.

3.3. Reprogrammed Carboxylate Interactions Display Unique Assembly/Disassembly Profiles. Analysis of the D77K and R46G/E50K/E97G CP assembly profiles identified that each has a unique environmental response. Specifically, the D77K mutation disassembles at pH 9, while the TMV and VLP E50Q/D77N rods remain assembled under this elevated pH condition (Figure 3A). Additionally, restoring the disassembled D77K CP solution to pH 7 solution conditions

results in the reassembly of the nanorods. Similarly, the R46G/E50K/E97G mutant CP also displays a unique disassembly behavior in response to ionic strength (Figure 3B). At low salt concentration the R46G/E50K/E97G CP disassembles but can then rapidly reassemble upon restoration of the solution's ionic strength. Interestingly, the conditions that trigger disassembly in each of these CP variants in solution is not shared by the other. D77K VLP nanorods are primarily affected by pH and not by ionic strength, while the R46G/E50K/E97G nanorods show disassembly only at low ionic strength with pH having little effect (Figure 4A,B). This variation in required assembly conditions makes these CPs potentially useful components for the controlled assembly of chimeric VLPs.

It is likely that the pH-based disassembly of D77K VLP results from the deprotonation and subsequent loss of positive charge of the lysine side chain's primary amine in alkaline conditions around pH 9. The pK_a of this amine group in a dilute solution of free lysine is ~ 10.5 .³³ However, this value can change considerably depending on the local microenvironment of the amine group in the folded protein and within the assembled rod. A similar deprotonation of the lysine in R46G/E50K/E97G CP may also occur; however, the partial neutralization of the lateral intersubunit interaction via the E97G substitution likely negates the impact of the engineered axial salt bridge, resulting in the relative stability of this CP at pH 9.

For the ionic-strength-based disassembly of R46G/E50K/E97G CP, structural modeling indicates that the predicted assembly promoting the salt bridge between the introduced lysine and the axially oriented carboxylate on the opposing subunit could be additionally stabilized by dissolved ions. While the side chain of the E50K substitution is thought to provide a stabilizing force when interacting with D77 of the opposing subunit, the E50K lysine is also positioned to interact with R71 of the opposing subunit, generating a repulsive interaction. This repulsive interaction may be mitigated by an ion screening effect when sufficient negative ions are present, allowing the ionic strength of the solution to control the assembly of this nanorod. The D77K lysine, however, does not interact across an intersubunit boundary with R71, and therefore VLP assembly would not be expected to depend on dissolved ions for charge screening.

3.4. Directed Assembly of Chimeric Nanorods. The unique pH and ionic-strength assembly profiles of D77K and R46G/E50K/E97G, respectively, were investigated as a means to produce chimeric virus particles. For these experiments, the D77K mutant was genetically labeled with a C-terminal HA peptide tag, while the R46G/E50K/E97G mutant was similarly labeled using a FLAG peptide tag. Solutions containing unlabeled TMV and modified CP VLPs were combined and dialyzed against solution conditions that promote disassembly of the modified CP VLPs. For D77K-HA VLP, this entailed dialysis to pH 9 and for R46G/E50K/E97G-FLAG dialysis against filtered water adjusted to pH 7. Disassembled CPs were then mixed with TMV virions and buffer conditions adjusted back to pH 7 or increased salinity (0.3 M NaCl) by dialysis to initiate reassembly of the D77K-HA or R46G/E50K/E97G-FLAG CP, respectively. Samples were then immunolabeled with anti-FLAG or anti-HA antibodies and imaged by electron microscopy.

Results from the coassembly of D77K-HA CP and TMV clearly show consistent and efficient assembly of D77K-HA CP

onto the unlabeled TMV (Figure 5A,B). The resulting hybrid unlabeled TMV–D77K-HA VLP nanorods showed a range of lengths and were selectively segregated into unlabeled and labeled sections by the anti-HA antibodies. It is likely that the strength of the mutant CP–CP interactions combined with CP concentration are factors affecting the observed length of the hybrid nanorod. In addition, such pH treatments have been shown to expose the 5' end of the viral RNA, which functions as a ribosome binding site during viral infection.²⁸ For determination of whether exposure of the 5' end of the virus RNA genome during dialysis plays a role in the coassembly of chimeric D77K-HA nanorods, RNase A was added to the TMV samples prior to coassembly and immunolabeling (Figure 5B). Results revealed the presence of similar end-assembled chimeric nanorods, indicating the genomic RNA is not required for the observed coassembly. For further determination of whether the viral genomic RNA contributes to the observed chimeric nanorod assembly, the D77K-HA CP was coassembled onto a RNA-free VLP produced by the neutralization of the lateral carboxylate cluster through CP amino acid substitutions E106Q/E95Q/E97Q/D109N. The D77K-HA was found to assemble onto the E106Q/E95Q/E97Q/D109N VLP in a manner similar to that observed using TMV virions or TMV RNase A-treated virions (Figure 5A–C). Thus, genomic viral RNA is not required for the coassembly of these CPs.

Coassembly of R46G/E50K/E97G-FLAG CP onto TMV by the depletion and subsequent replenishment of dissolved ions also produced chimeric nanorods (Figure 5C). Interestingly, washing the electron microscopy grids containing the coassembled TMV - R46G/E50K/E97G-FLAG CP with deionized water pH 7 resulted in the R46G/E50K/E97G-FLAG CP section exhibiting a loose and fragmented structure consistent with its disassembly at low ionic-strength conditions (Figure 5D). Combined these results indicate that carboxylate alterations can be used in the controlled assembly and disassembly of chimeric VLPs.

3.5. Surface-Bound Fabrication of Coassembled Nanoparticles. The ability of D77K-HA and R46G/E50K/E97G-FLAG CPs to coassemble onto a surface-attached TMV base layer in a condition-dependent manner was also investigated. For these studies, gold-coated silicon wafer chips were spotted with 3 μ L of 0.1 mg/mL TMV1cys virus (Figure 6A). TMV1cys encodes a novel cysteine residue within its N-terminal arm that has been demonstrated to function in the attachment of the virus onto gold surfaces.³⁴ Specifically, the added cysteine thiol group is surface-exposed only on the TMV rod ends, allowing for the formation of thiol–gold bonds that attach one end of the virus rod to the gold surface, leaving the other end exposed for further modification. TMV1cys-spotted chips were incubated in 1 mL of Tris buffer saline (0.2 M NaCl), pH 7, followed by the addition of 20 μ L of 0.5 μ g of D77K-HA CP, disassembled by dialysis in pH 9 Tris buffer, or R46G/E50K/E97G-FLAG CP, disassembled by dialysis in pH 7 deionized water. Added CPs were incubated overnight at room temperature to permit coassembly onto surface-attached TMV1cys. Coassembled chips were incubated overnight in either Tris buffer saline (0.2 M NaCl), pH 7 or pH 9, or with deionized water, pH 7. Chips were then washed and incubated in Tris buffer saline with primary-tag-specific antibody (FLAG or HA) followed by the addition of a secondary alkaline phosphatase conjugated antibody and finally the addition of a

substrate, resulting in the production of a dark precipitant on the surface of the gold-coated chip.

Results demonstrate both D77K-HA and R46G/E50K/E97G-FLAG CPs maintain their pH and ion concentration dependent assembly and disassembly features when coassembled onto surface-attached TMV1cys nanorods (Figure 6B,C). Importantly, surface-assembled D77K-HA CP was responsive only to the pH and not to the ionic strength, while assembly of the R46G/E50K/E97G-FLAG CP was affected only by the ionic strength and not the pH. Thus, these CPs maintain their solution assembly behaviors when coassembled on surface-attached TMV1cys nanorods.

Sequential assemblies composed of surface-attached TMV1cys coassembled first with either D77K-HA and second with R46G/E50K/E97G-FLAG CPs or first with R46G/E50K/E97G-FLAG and second with D77K-HA CPs were also investigated as a means to control the layering of specific CPs. For confirmation of sequential assembly, individual chips were washed under buffer conditions that promote the disassembly of the first coassembled CP layer, deionized water for R46G/E50K/E97G-FLAG or pH 9 for D77K. Washed chips were then probed using antibodies against the second coassembled CP. Results demonstrate the sequential assembly of R46G/E50K/E97G-FLAG and D77K onto surface-attached TMV1cys (Figure 7A,B). This layering is confirmed by the ability of wash conditions specific for the disassembly of the first assembled CP layer to remove the second CP layer (Figure 7A,B). Thus, the unique assembly behaviors of the R46G/E50K/E97G-FLAG and D77K CPs can be used to control the layering of functionally distinct CP assemblies.

4. CONCLUSION

TMV controls its assembly and disassembly via defined intersubunit carboxyl–carboxylate interactions whose charge-based repulsion functions as an environmental sensor and virion stability switch.^{16,29} Thus, such carboxylate interactions represent ideal sites from which to reprogram these intersubunit interactions with novel environmental responses aimed at controlling nanorod assembly and stability. In this study, knowledge of the native structure and mechanism by which TMV regulates assembly were used to impart the viral CP with novel assembly and disassembly triggers. Specifically, modifications to the axial as well as lateral carboxylate interactions demonstrate the malleability of the TMV CP for the engineering of novel intersubunit interactions that can confer environmentally unique assembly–disassembly behaviors. The unique properties and behaviors of these novel VLP-forming CPs represent a distinctive set of reagents that can be further exploited to drive higher-order assembly behaviors for the generation of TMV-based nanoparticles with enhanced structural and functional complexities.

AUTHOR INFORMATION

Corresponding Author

James N. Culver – *Institute for Bioscience and Biotechnology Research, Department of Plant Science and Landscape Architecture, University of Maryland, College Park, Maryland 20742, United States*; orcid.org/0000-0003-0623-3369; Email: jculver@umd.edu

Authors

Adam D. Brown – *Fischell Department of Bioengineering, University of Maryland, College Park, Maryland 20742, United States*

Sangwook Chu – *Institute for Systems Research, University of Maryland, College Park, Maryland 20742, United States*; orcid.org/0000-0002-1173-6377

Madhu Kappagantu – *Institute for Bioscience and Biotechnology Research, University of Maryland, College Park, Maryland 20742, United States*

Reza Ghodssi – *Institute for Systems Research, Department of Electrical and Computer Engineering, University of Maryland, College Park, Maryland 20742, United States*

Complete contact information is available at:
<https://pubs.acs.org/10.1021/acs.biomac.1c00258>

Notes

The authors declare no competing financial interest.

ACKNOWLEDGMENTS

This work was funded by the Biochemistry Program of the Army Research Office (W911NF-17-1-0137). The authors also thank Professor Donald L. D. Caspar, Florida State University, for sharing his expertise on the structural assembly of TMV.

REFERENCES

- (1) Culver, J. N.; Brown, A. D.; Zang, F.; Gnerlich, M.; Gerasopoulos, K.; Ghodssi, R. Plant virus directed fabrication of nanoscale materials and devices. *Virology* **2015**, *479–480*, 200–12.
- (2) Steinmetz, N. F.; Lim, S.; Sainsbury, F. Protein cages and virus-like particles: from fundamental insight to biomimetic therapeutics. *Biomater. Sci.* **2020**, *8* (10), 2771–2777.
- (3) Chen, Z.; Li, N.; Li, S. B.; Dharmawardana, M.; Schlimme, A.; Gassensmith, J. J. Viral chemistry: the chemical functionalization of viral architectures to create new technology. *Wires Nanomed Nanobi* **2016**, *8* (4), 512–534.
- (4) Eiben, S.; Koch, C.; Altintoprak, K.; Southan, A.; Tovar, A.; Laschat, S.; Weiss, I. M.; Wege, C. Plant virus-based materials for biomedical applications: Trends and prospects. *Adv. Drug Delivery Rev.* **2019**, *145*, 96–118.
- (5) Hong, F.; Zhang, F.; Liu, Y.; Yan, H. DNA Origami: Scaffolds for Creating Higher Order Structures. *Chem. Rev.* **2017**, *117* (20), 12584–12640.
- (6) Pfeifer, W.; Sacca, B. From Nano to Macro through Hierarchical Self-Assembly: The DNA Paradigm. *ChemBioChem* **2016**, *17* (12), 1063–1080.
- (7) King, N. P.; Lai, Y. T. Practical approaches to designing novel protein assemblies. *Curr. Opin. Struct. Biol.* **2013**, *23* (4), 632–8.
- (8) Rothmund, P. W. Folding DNA to create nanoscale shapes and patterns. *Nature* **2006**, *440* (7082), 297–302.
- (9) Schwarz, B.; Uchida, M.; Douglas, T. Biomedical and Catalytic Opportunities of Virus-Like Particles in Nanotechnology. *Adv. Virus Res.* **2017**, *97*, 1–60.
- (10) Wen, A. M.; Steinmetz, N. F. Design of virus-based nanomaterials for medicine, biotechnology, and energy. *Chem. Soc. Rev.* **2016**, *45* (15), 4074–126.
- (11) Fan, X. Z.; Pomerantseva, E.; Gnerlich, M.; Brown, A.; Gerasopoulos, K.; McCarthy, M.; Culver, J.; Ghodssi, R. Tobacco mosaic virus: A biological building block for micro/nano/bio systems. *J. Vac. Sci. Technol., A* **2013**, *31* (5), 050815.
- (12) Strable, E.; Finn, M. G. Chemical Modification of Viruses and Virus-Like Particles. *Curr. Top. Microbiol. Immunol.* **2009**, *327*, 1–21.
- (13) Lomonosoff, G. P.; Wege, C. TMV Particles: The Journey From Fundamental Studies to Bionanotechnology Applications. *Adv. Virus Res.* **2018**, *102*, 149–176.

- (14) Bhokisham, N.; Liu, Y.; Brown, A. D.; Payne, G. F.; Culver, J. N.; Bentley, W. E. Transglutaminase-mediated assembly of multi-enzyme pathway onto TMV brush surfaces for synthesis of bacterial autoinducer-2. *Biofabrication* **2020**, *12* (4), 045017.
- (15) Sachse, C.; Chen, J. Z.; Coureux, P. D.; Stroupe, M. E.; Fandrich, M.; Grigorieff, N. High-resolution electron microscopy of helical specimens: A fresh look at Tobacco Mosaic Virus. *J. Mol. Biol.* **2007**, *371* (3), 812–835.
- (16) Namba, K.; Pattanayek, R.; Stubbs, G. Visualization of protein-nucleic acid interactions in a virus - refined structure of intact tobacco mosaic virus at 2.9 Å resolution by X-ray fiber diffraction. *J. Mol. Biol.* **1989**, *208* (2), 307–325.
- (17) Bhyravbhata, B.; Watowich, S. J.; Caspar, D. L. D. Refined atomic model of the four-layer aggregate of the tobacco mosaic virus coat protein at 2.4-angstrom resolution. *Biophys. J.* **1998**, *74* (1), 604–615.
- (18) Bloomer, A. C.; Champness, J. N.; Bricogne, G.; Staden, R.; Klug, A. Protein disk of tobacco mosaic virus at 2.8 Å resolution showing the interactions within and between subunits. *Nature* **1978**, *276* (5686), 362–8.
- (19) Dedeo, M. T.; Duderstadt, K. E.; Berger, J. M.; Francis, M. B. Nanoscale protein assemblies from a circular permutant of the tobacco mosaic virus. *Nano Lett.* **2010**, *10* (1), 181–6.
- (20) Zhou, K.; Li, F.; Dai, G. L.; Meng, C.; Wang, Q. B. Disulfide Bond: Dramatically Enhanced Assembly Capability and Structural Stability of Tobacco Mosaic Virus Nanorods. *Biomacromolecules* **2013**, *14* (8), 2593–2600.
- (21) Wege, C.; Koch, C. From stars to stripes: RNA-directed shaping of plant viral protein templates-structural synthetic virology for smart biohybrid nanostructures. *Wiley Interdiscip. Rev.: Nanomed. Nanobiotechnol.* **2020**, *12* (2), e1591.
- (22) Mueller, A.; Eber, F. J.; Azucena, C.; Petershans, A.; Bittner, A. M.; Gliemann, H.; Jeske, H.; Wege, C. Inducible site-selective bottom-up assembly of virus-derived nanotube arrays on RNA-equipped wafers. *ACS Nano* **2011**, *5* (6), 4512–20.
- (23) Geiger, F. C.; Eber, F. J.; Eiben, S.; Mueller, A.; Jeske, H.; Spatz, J. P.; Wege, C. TMV nanorods with programmed longitudinal domains of differently addressable coat proteins. *Nanoscale* **2013**, *5* (9), 3808–16.
- (24) Schneider, A.; Eber, F. J.; Wenz, N. L.; Altintoprak, K.; Jeske, H.; Eiben, S.; Wege, C. Dynamic DNA-controlled "stop-and-go" assembly of well-defined protein domains on RNA-scaffolded TMV-like nanotubes. *Nanoscale* **2016**, *8* (47), 19853–19866.
- (25) Eber, F. J.; Eiben, S.; Jeske, H.; Wege, C. RNA-controlled assembly of tobacco mosaic virus-derived complex structures: from nanoboomerangs to tetrapods. *Nanoscale* **2015**, *7* (1), 344–355.
- (26) Brown, A. D.; Naves, L.; Wang, X.; Ghodssi, R.; Culver, J. N. Carboxylate-Directed In Vivo Assembly of Virus-like Nanorods and Tubes for the Display of Functional Peptides and Residues. *Biomacromolecules* **2013**, *14* (9), 3123–9.
- (27) Culver, J. N.; Dawson, W. O.; Plonk, K.; Stubbs, G. Site-Directed Mutagenesis Confirms the Involvement of Carboxylate Groups in the Disassembly of Tobacco Mosaic-Virus. *Virology* **1995**, *206* (1), 724–730.
- (28) Lu, B.; Stubbs, G.; Culver, J. N. Carboxylate interactions involved in the disassembly of tobacco mosaic tobamovirus. *Virology* **1996**, *225* (1), 11–20.
- (29) Caspar, D. L. D. Assembly and stability of the tobacco mosaic virus particle. *Adv. Protein Chem.* **1964**, *18*, 37–123.
- (30) Culver, J. N. Tobacco mosaic virus assembly and disassembly: Determinants in pathogenicity and resistance. *Annu. Rev. Phytopathol.* **2002**, *40*, 287–308.
- (31) Zang, F.; Gerasopoulos, K.; Brown, A. D.; Culver, J. N.; Ghodssi, R. Capillary Microfluidics-Assembled Virus-like Particle Bionanoreceptor Interfaces for Label-Free Biosensing. *ACS Appl. Mater. Interfaces* **2017**, *9* (10), 8471–8479.
- (32) Culver, J. N.; Dawson, W. O.; Plonk, K.; Stubbs, G. Site-directed mutagenesis confirms the involvement of carboxylate groups in the disassembly of tobacco mosaic virus. *Virology* **1995**, *206* (1), 724–730.
- (33) Stryer, L.; Berg, J. M.; Tymoczko, J. L. *Biochemistry*, 5th ed.; Freeman, W.H.: New York, 2002.
- (34) Royston, E.; Ghosh, A.; Kofinas, P.; Harris, M. T.; Culver, J. N. Self-assembly of virus-structured high surface area nanomaterials and their application as battery electrodes. *Langmuir* **2008**, *24* (3), 906–12.